PARAFAC-Based Time-Varying Channel Estimation for IRS-Aided Communications

Kenneth B. A. Benício, André L. F. de Almeida, Bruno Sokal, Fazal-E-Asim, Behrooz Makki, and Gabor Fodor

Abstract—This paper proposes a tensor-based parametric channel estimation technique for IRS-assisted communication systems with time-varying channel parameters. We exploit the multidimensional structure of the received signal by developing a 3rd-order PARAFAC tensor model that is solved by employing the iteratively ALS algorithm. Our simulation results show that the proposed approach provides enhanced performance in terms of NMSE of the concatenated channel compared to the competing solutions by capitalizing on the intrinsic tensor structure of the received signal without increasing the computational complexity of the channel estimation.

Keywords—channel estimation, intelligent reflecting surfaces, tensor-based algorithm, complexity analysis

I. INTRODUCTION

With the increasing number of users due to the implementation of the fifth generation (5G) and beyond fifth generation (B5G), there is a growing demand for network resources in terms of either energy or spectrum usage [1]. Most of the recent works concentrate on solving problems of cooperative relaying, beamforming design, or resource allocation either at the user equipment (UE) or at the base station (BS) [2], [3]. However, the propagation environment remains an unknown factor not accounted for in formulating these problems [4].

In this context, intelligent reflecting surface (IRS) has been explored as one of the possible technologies for integration into B5G and sixth generation (6G) wireless networks aimed at realizing crucial functionalities such as system integration and data transmission [5]. This interest arises from the potential of IRS to enhance network coverage and establish an intelligent propagation environment [6]–[8]. An IRS is a two-dimensional panel composed of many passive reflecting elements and a smart controller, which controls the reflecting elements to independently change the phase shifts of impinging electromagnetic waves to smartly maximize the signal-to-noise ratio (SNR) by adding them constructively or destructively at the intended receiver [4]. As IRS operates as a passive structure, its power consumption primarily arises from the operation of the smart controller, which lacks the capability to process or amplify incoming signals.

Since the IRS usually is composed of passive elements, it is unable to employ signal processing techniques to the impinging signals, meaning that channel estimation techniques must be carried out at the end nodes of the network, either the BS or the UE, by transmitting pilot signals according to a training protocol. Several works have already addressed this problem, as the ones mentioned in [9]–[11].

In [9], to perform supervised parameter estimation, a tensor approach is employed, in which the decoupling of the BS-IRS and IRS-UE channels is achieved by modeling the received signal at the BS as a 3rd order PARAFAC tensor. In our previous work [10], we proposed a 3th order Tucker to solve the problem of parameter estimation of (quasi)-static channels in the context of an IRS-aided multiple input multiple output (MIMO) system. The problem was solved by employing the high order single value decomposition (HOSVD) and alternating least squares (ALS) algorithms with no increase in computational complexity compared to the competing methods. Also, in [11], we proposed a scenario for data-aided tracking where all involved channels were time-varying. This was solved by employing tensor methods on a two-stage parameter estimation framework. In this work, we consider that the IRS and the BS are in fixed positions, which is more realistic, meaning that the BS-IRS channel is static.

In this paper, we propose a tensor modeling for the received signal at the BS that models the signal as a 3rd order PARAFAC tensor to solve the parameter estimation problem by employing the ALS algorithm [12] in the context of a single time-varying channel. Different from our approach in [11], this new solution solves the problem by developing a model that exploits the fact that the channel between the BS and the IRS is static. Usually, this is an acceptable consideration since the BS and the IRS are deployed in fixed positions. We also provide system design recommendations for our proposed solution while discussing the computational complexity of the proposed solution. Our simulation results show that the proposed tensor-based solution achieves better performance in terms of normalized mean square error (NMSE) of the concatenated channel as the classical least squares (LS) filter and the proposed Khatri-Rao factorization (KRF) in [9] without increasing the computational complexity.

Notation: Scalars, vectors, matrices, and tensors are represented as $a, \boldsymbol{a}, \boldsymbol{A}$, and $\mathcal{A}$. Also, $\boldsymbol{A}^*$, $\boldsymbol{A}^{\mathrm{T}}$, $\boldsymbol{A}^{\mathrm{H}}$, and $\boldsymbol{A}^\dagger$ stand for the conjugate, transpose, Hermitian, and pseudo-inverse, of a matrix $\boldsymbol{A}$, respectively. The jth column of $\boldsymbol{A} \in \mathbb{C}^{I \times J}$ is denoted by $\boldsymbol{a}_j \in \mathbb{C}^{I \times 1}$. The operator $\mathrm{vec}(\cdot)$ transforms a matrix into a vector by stacking its columns, e.g., $\mathrm{vec}(\boldsymbol{A}) = \boldsymbol{a} \in \mathbb{C}^{IJ \times 1}$, while the $\mathrm{unvec}(\cdot)_{I \times J}$ operator undo the operation. The operator $\mathrm{D}(\cdot)$ converts a vector into a diagonal matrix, $\mathrm{D}_j(\boldsymbol{B})$ forms a diagonal matrix $R \times R$ out of the jth row of $\boldsymbol{B} \in \mathbb{C}^{J \times R}$. Also, $\boldsymbol{I}_N$ denotes an identity matrix of size $N \times N$. The symbols $\otimes$ and $\diamond$ indicate the Kronecker and Khatri-Rao products.
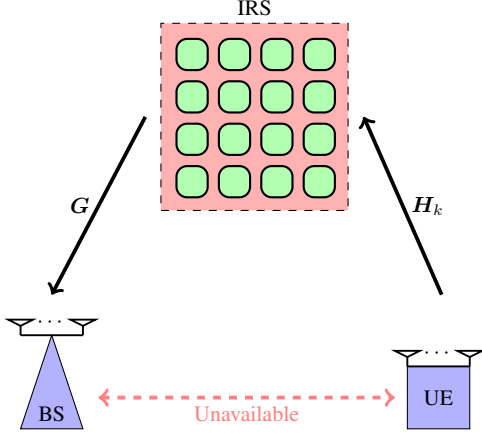
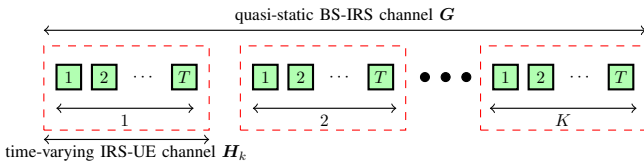Fig. 1: Proposed IRS-assisted MIMO system scenario.

Fig. 2: Time-domain transmission protocol.

II. SYSTEM MODEL

We consider an uplink IRS-assisted MIMO scenario with a BS equipped with M receiver antennas, which receives a signal from a UE equipped with Q transmit antennas *via* a passive IRS with N reflecting elements as shown in Fig. 1. The transmission protocol contains $K+1$ blocks each of length of T symbol periods, as shown in Fig 2. The received signal is given by

$$\boldsymbol{y}_{k,t} = \boldsymbol{G}\mathrm{D}(\boldsymbol{s}_t)\boldsymbol{H}_k\boldsymbol{z}_t + \boldsymbol{v}_{k,t} \in \mathbb{C}^{M\times 1}, \quad (1)$$

where $\mathrm{D}(\boldsymbol{s}_t)$ is the IRS phase-shift matrix, $\boldsymbol{z}_t$ is the pilot sequence and $\boldsymbol{v}_{k,t}$ is the additive white Gaussian noise (AWGN) vector with $t \in \{1, \cdots, T\}$. We assume that the IRS-UE link changes faster due to mobility while the BS-IRS remains static. Specifically, the IRS-UE channel $\boldsymbol{H}_k$ changes between blocks, while the BS-IRS channel $\boldsymbol{G}$ remains constant during $K+1$ blocks. Assuming a millimeter Wave (mmWave) scenario, we adopt a multipath channel model [13] for the involved channels. We can express these channel matrices as follows

$$\boldsymbol{G} = \sum_{l_1=1}^{L_1} \alpha^{(l_1)}\boldsymbol{a}_{\mathrm{r_x}}(\mu_{\mathrm{bs}}^{(l_1)})\boldsymbol{b}_{\mathrm{t_x}}^{(\mathrm{irs})\mathrm{H}}(\mu_{\mathrm{irs_D}}^{(l_1)}, \psi_{\mathrm{irs_D}}^{(l_1)}), \quad (2)$$

$$\boldsymbol{H}_k = \sum_{l_2=1}^{L_2} \beta_k^{(l_2)}\boldsymbol{b}_{\mathrm{r_x}}^{(\mathrm{irs})}(\mu_{\mathrm{irs_A}}^{(l_2)}, \psi_{\mathrm{irs_A}}^{(l_2)})\boldsymbol{a}_{\mathrm{t_x}}^{\mathrm{H}}(\mu_{\mathrm{ue}}^{(l_2)}), \quad (3)$$

where L_1 and L_2 are the number of directions for channels $\boldsymbol{G}$ and $\boldsymbol{H}_k$, respectively. The lth BS steering vector $\boldsymbol{a}_{\mathrm{r_x}}(\mu_{\mathrm{bs}}^{(l_1)})$ is associated with the spatial frequency $\mu_{\mathrm{bs}}^{(l_1)} = \pi\cos(\phi_{\mathrm{bs}}^{(l_1)})$, with $\phi_{\mathrm{bs}}^{(l_1)}$ being the angle of arrival (AoA), which can be further written as

$$\boldsymbol{a}_{\mathrm{r_x}}(\mu_{\mathrm{bs}}^{(l_1)}) = \left[1, \cdots, e^{-j(M-1)\mu_{\mathrm{bs}}^{(l_1)}}\right]^{\mathrm{T}} \in \mathbb{C}^{M\times 1}. \quad (4)$$

Similarly, the pth one-dimensional steering vector for the UE is $\boldsymbol{a}_{\mathrm{t_x}}(\mu_{\mathrm{ue}}^{(l_2)})$ having spatial frequency, which is defined as $\mu_{\mathrm{ue}}^{(l_2)} = \pi\cos(\phi_{\mathrm{ue}}^{(l_2)})$, with $\phi_{\mathrm{ue}}^{(l_2)}$ being the angle of departure (AoD), and can be written in terms of spatial frequency as

$$\boldsymbol{a}_{\mathrm{t_x}}(\mu_{\mathrm{ue}}^{(l_2)}) = \left[1, \cdots, e^{-j(Q-1)\mu_{\mathrm{ue}}^{(l_2)}}\right]^{\mathrm{T}} \in \mathbb{C}^{Q\times 1}. \quad (5)$$

At the IRS, $\boldsymbol{b}_{\mathrm{r_x}}^{(\mathrm{irs})}(\mu_{\mathrm{irs_A}}^{(l_2)}, \psi_{\mathrm{irs_A}}^{(l_2)})$ is the 2D steering vector with spatial frequencies $\mu_{\mathrm{irs_A}}^{(l_2)} = \pi\cos(\phi_{\mathrm{irs_A}}^{(l_2)})\sin(\theta_{\mathrm{irs_A}}^{(l_2)})$ and $\psi_{\mathrm{irs_A}}^{(l_2)} = \pi\cos(\phi_{\mathrm{irs_A}}^{(l_2)})$, where $\phi_{\mathrm{irs_A}}^{(l_2)}$ and $\theta_{\mathrm{irs_A}}^{(l_2)}$ are the azimuth AoA and the elevation AoA, respectively. This can be further written as the Kronecker product between two steering vectors as

$$\boldsymbol{b}_{\mathrm{r_x}}^{(\mathrm{irs})}(\mu_{\mathrm{irs_A}}^{(l_2)}, \psi_{\mathrm{irs_A}}^{(l_2)}) = \boldsymbol{b}_{\mathrm{r_x}}^{(\mathrm{irs})}(\mu_{\mathrm{irs_A}}^{(l_2)}) \otimes \boldsymbol{b}_{\mathrm{r_x}}^{(\mathrm{irs})}(\psi_{\mathrm{irs_A}}^{(l_2)}) \in \mathbb{C}^{N\times 1}. \quad (6)$$

The IRS transmission steering vector, $\boldsymbol{b}_{\mathrm{t_x}}^{(\mathrm{irs})}(\mu_{\mathrm{irs_D}}^{(l_1)}, \psi_{\mathrm{irs_D}}^{(l_1)})$, with spatial frequencies defined as $\mu_{\mathrm{irs_D}}^{(l_1)} = \pi\cos(\phi_{\mathrm{irs_D}}^{(l_1)})\sin(\theta_{\mathrm{irs_D}}^{(l_1)})$ and $\psi_{\mathrm{irs_D}}^{(l_1)} = \pi\cos(\phi_{\mathrm{irs_D}}^{(l_1)})$, where $\phi_{\mathrm{irs_D}}^{(l_1)}$ and $\theta_{\mathrm{irs_D}}^{(l_1)}$ are respectively the azimuth AoD and the elevation AoD, is given by

$$\boldsymbol{b}_{\mathrm{t_x}}^{(\mathrm{irs})}(\mu_{\mathrm{irs_D}}^{(l_1)}, \psi_{\mathrm{irs_D}}^{(l_1)}) = \boldsymbol{b}_{\mathrm{t_x}}^{(\mathrm{irs})}(\mu_{\mathrm{irs_D}}^{(l_1)}) \otimes \boldsymbol{b}_{\mathrm{t_x}}^{(\mathrm{irs})}(\psi_{\mathrm{irs_D}}^{(l_1)}) \in \mathbb{C}^{N\times 1}. \quad (7)$$

The IRS phase-shift vector is defined as $\boldsymbol{s}_t = \left[e^{j\theta_{1,t}}, \cdots, e^{j\theta_{N,t}}\right]^{\mathrm{T}} \in \mathbb{C}^{N\times 1}$, where $\theta_{n,t}$ is the phase-shift of the nth IRS element at the tth time slot. Moreover, $\boldsymbol{\alpha} = [\alpha^{(1)}, \cdots, \alpha^{(L_1)}]^{\mathrm{T}} \in \mathbb{C}^{L_1\times 1}$ and $\boldsymbol{\beta}_k = [\beta_k^{(1)}, \cdots, \beta_k^{(L_2)}]^{\mathrm{T}} \in \mathbb{C}^{L_2\times 1}$ collect the path loss and fading components of the BS-IRS and IRS-UE links, respectively. The aging effects are modeled by assuming that $\boldsymbol{\beta}_k \in \mathbb{C}^{L_2\times 1}$ vary according to a first-order auto-regressive (AR) process defined as [14]

$$\boldsymbol{\beta}_k = \lambda\boldsymbol{\beta}_k + \boldsymbol{\xi}_k, k = \{1, \cdots, K\}, \quad (8)$$

where $\boldsymbol{\xi}_k \sim \mathcal{CN}(\boldsymbol{0}, (1-\lambda^2)\boldsymbol{I}_{L_2}) \in \mathbb{C}^{L_2\times 1}$ is the AR process noise term for the IRS-UE link with λ being its correlation coefficient [15]. We can compact the notation for $\boldsymbol{G}$ and $\boldsymbol{H}_k$ as follows

$$\boldsymbol{G} = \boldsymbol{A}_{\mathrm{r_x}}\boldsymbol{D}(\boldsymbol{\alpha})\boldsymbol{B}_{\mathrm{t_x}}^{\mathrm{H}} \in \mathbb{C}^{M\times N}, \quad (9)$$

$$\boldsymbol{H}_k = \boldsymbol{B}_{\mathrm{r_x}}\boldsymbol{D}(\boldsymbol{\beta}_k)\boldsymbol{A}_{\mathrm{t_x}}^{\mathrm{H}} \in \mathbb{C}^{N\times Q}, \quad (10)$$

where $\boldsymbol{A}_{\mathrm{r_x}}$, $\boldsymbol{A}_{\mathrm{t_x}}$, $\boldsymbol{B}_{\mathrm{r_x}}$, and $\boldsymbol{B}_{\mathrm{t_x}}$ are the steering matrices defined as

$$\boldsymbol{A}_{\mathrm{r_x}} = \left[\boldsymbol{a}_{\mathrm{r_x}}(\mu_{\mathrm{bs}}^{(1)}), \cdots, \boldsymbol{a}_{\mathrm{r_x}}(\mu_{\mathrm{bs}}^{(L_1)})\right] \in \mathbb{C}^{M\times L_1},$$

$$\boldsymbol{A}_{\mathrm{t_x}} = \left[\boldsymbol{a}_{\mathrm{t_x}}(\mu_{\mathrm{ue}}^{(1)}), \cdots, \boldsymbol{a}_{\mathrm{t_x}}(\mu_{\mathrm{ue}}^{(L_2)})\right] \in \mathbb{C}^{Q\times L_2},$$

$$\boldsymbol{B}_{\mathrm{r_x}} = \left[\boldsymbol{b}_{\mathrm{r_x}}^{(\mathrm{irs})}(\mu_{\mathrm{irs_A}}^{(1)}, \psi_{\mathrm{irs_A}}^{(1)}), \cdots, \boldsymbol{b}_{\mathrm{r_x}}^{(\mathrm{irs})}(\mu_{\mathrm{irs_A}}^{(L_2)}, \psi_{\mathrm{irs_A}}^{(L_2)})\right] \in \mathbb{C}^{N\times L_2},$$

$$\boldsymbol{B}_{\mathrm{t_x}} = \left[\boldsymbol{b}_{\mathrm{t_x}}^{(\mathrm{irs})}(\mu_{\mathrm{irs_D}}^{(1)}, \psi_{\mathrm{irs_D}}^{(1)}), \cdots, \boldsymbol{b}_{\mathrm{t_x}}^{(\mathrm{irs})}(\mu_{\mathrm{irs_D}}^{(L_1)}, \psi_{\mathrm{irs_D}}^{(L_1)})\right] \in \mathbb{C}^{N\times L_1}.$$

III. PARAFAC-BASED PILOT SIGNAL DESIGN

This section describes the proposed tensor-based method for channel parameter estimation exploiting a 3rd order PARAFAC tensor. Using properties $\mathrm{vec}(\boldsymbol{ABC}) = (\boldsymbol{C}^{\mathrm{T}} \otimes \boldsymbol{A})\mathrm{vec}(\boldsymbol{B})$ and $\mathrm{vec}(\boldsymbol{AD}(\boldsymbol{b})\boldsymbol{C}) = (\boldsymbol{C}^{\mathrm{T}} \diamond \boldsymbol{A})\boldsymbol{b}$ in the signal model of (1), yields

$$\begin{aligned} \boldsymbol{y}_{k,t} &= \mathrm{vec}\left(\boldsymbol{I}_M\boldsymbol{G}\mathrm{D}(\boldsymbol{s}_t)\boldsymbol{H}_k\boldsymbol{z}_t\right) + \boldsymbol{v}_{k,t} \in \mathbb{C}^{M\times 1}, \\ &= (\boldsymbol{z}_t^{\mathrm{T}} \otimes \boldsymbol{I}_M)\mathrm{vec}(\boldsymbol{G}\mathrm{D}(\boldsymbol{s}_t)\boldsymbol{H}_k) + \boldsymbol{v}_{k,t}, \\ &= (\boldsymbol{s}_t^{\mathrm{T}} \otimes \boldsymbol{z}_t^{\mathrm{T}} \otimes \boldsymbol{I}_M)\mathrm{vec}(\boldsymbol{H}_k^{\mathrm{T}} \diamond \boldsymbol{G}) + \boldsymbol{v}_{k,t}. \end{aligned} \quad (11)$$

and applying again property $\text{vec}(\boldsymbol{ABC}) = (\boldsymbol{C}^{\text{T}} \otimes \boldsymbol{A})\text{vec}(\boldsymbol{B})$ give us

$$
\begin{aligned}
\boldsymbol{y}_{k,t} &= \text{vec}[(\boldsymbol{z}_t^{\text{T}} \otimes \boldsymbol{I}_M)(\boldsymbol{H}_k^{\text{T}} \diamond \boldsymbol{G})\boldsymbol{s}_t] + \boldsymbol{v}_{k,t}, \\
&= (\boldsymbol{s}_t^{\text{T}} \otimes \boldsymbol{z}_t^{\text{T}} \otimes \boldsymbol{I}_M)\text{vec}(\boldsymbol{H}_k^{\text{T}} \diamond \boldsymbol{G}) + \boldsymbol{v}_{k,t}. \quad (12)
\end{aligned}
$$

Collecting the signals during the T symbol periods yields

$$
\begin{aligned}
\boldsymbol{y}_k &= \left[\boldsymbol{y}_{k,1}^{\text{T}}, \cdots, \boldsymbol{y}_{k,T}^{\text{T}}\right]^{\text{T}}, \quad &(13) \\
&= [(\boldsymbol{S} \diamond \boldsymbol{Z})^{\text{T}} \otimes \boldsymbol{I}_M]\text{vec}(\boldsymbol{H}_k^{\text{T}} \diamond \boldsymbol{G}) + \boldsymbol{v}_k \in \mathbb{C}^{MT \times 1}, \quad &(14) \\
&= \boldsymbol{\Omega}\boldsymbol{u}_k + \boldsymbol{v}_k \in \mathbb{C}^{MT \times 1}, \quad &(15)
\end{aligned}
$$

where $\boldsymbol{S} = [\boldsymbol{s}_1, \cdots, \boldsymbol{s}_T] \in \mathbb{C}^{N \times T}$, $\boldsymbol{Z} = [\boldsymbol{z}_1, \cdots, \boldsymbol{z}_T] \in \mathbb{C}^{Q \times T}$ are matrices collecting the IRS phase-shifts and pilots, $\boldsymbol{\Omega} = (\boldsymbol{S} \diamond \boldsymbol{Z})^{\text{T}} \otimes \boldsymbol{I}_M \in \mathbb{C}^{MT \times MQN}$, $\boldsymbol{u}_k = \text{vec}(\boldsymbol{H}_k^{\text{T}} \diamond \boldsymbol{G}) \in \mathbb{C}^{MQN \times 1}$, and $\boldsymbol{v}_k = \left[\boldsymbol{v}_{k,1}^{\text{T}}, \cdots, \boldsymbol{v}_{k,T}^{\text{T}}\right]^{\text{T}} \in \mathbb{C}^{MT \times 1}$ is the AWGN term. From (15), we formulate the following LS problem

$$
\hat{\boldsymbol{u}}_k = \arg \min_{\boldsymbol{u}_k} ||\boldsymbol{y}_k - \boldsymbol{\Omega}\boldsymbol{u}_k||_2^2, \quad (16)
$$

where the solution requires $T \geq QN$ and is given by

$$
\hat{\boldsymbol{u}}_k = \boldsymbol{\Omega}^{\dagger}\boldsymbol{y}_k \in \mathbb{C}^{MQN \times 1}. \quad (17)
$$

Let us define $\boldsymbol{R}_k = \text{unvec}_{MQ \times N}(\hat{\boldsymbol{u}}_k) \approx \boldsymbol{H}_k^{\text{T}} \diamond \boldsymbol{G} \in \mathbb{C}^{MQ \times N}$. Using (9) and (10), while applying property $(\boldsymbol{A} \otimes \boldsymbol{B})(\boldsymbol{C} \diamond \boldsymbol{D}) = (\boldsymbol{AC}) \diamond (\boldsymbol{BD})$, we have

$$
\begin{aligned}
\boldsymbol{R}_k &\approx [\boldsymbol{A}_{\text{tx}}^* \text{D}(\boldsymbol{\beta}_k)\boldsymbol{B}_{\text{rx}}^{\text{T}}] \diamond [\boldsymbol{A}_{\text{rx}}\text{D}(\boldsymbol{\alpha})\boldsymbol{B}_{\text{tx}}^{\text{H}}], \quad &(18) \\
&\approx (\boldsymbol{A}_{\text{tx}}^* \otimes \boldsymbol{A}_{\text{rx}})[(\text{D}(\boldsymbol{\beta}_k)\boldsymbol{B}_{\text{rx}}^{\text{T}}) \diamond (\text{D}(\boldsymbol{\alpha})\boldsymbol{B}_{\text{tx}}^{\text{H}})], \quad &(19) \\
&\approx (\boldsymbol{A}_{\text{tx}}^* \otimes \boldsymbol{A}_{\text{rx}})[\text{D}(\boldsymbol{\beta}_k) \otimes \text{D}(\boldsymbol{\alpha})](\boldsymbol{B}_{\text{rx}}^{\text{T}} \diamond \boldsymbol{B}_{\text{tx}}^{\text{H}}). \quad &(20)
\end{aligned}
$$

Let us consider $\boldsymbol{f}_k = \boldsymbol{\beta}_k \otimes \boldsymbol{\alpha} \in \mathbb{C}^{L_1 L_2 \times 1}$, then (20) can be rewritten as

$$
\boldsymbol{R}_k \approx \boldsymbol{A}\text{D}(\boldsymbol{f}_k)\boldsymbol{B}^{\text{T}} \in \mathbb{C}^{MQ \times N}, \quad (21)
$$

where $\boldsymbol{A} = (\boldsymbol{A}_{\text{tx}}^* \otimes \boldsymbol{A}_{\text{rx}}) \in \mathbb{C}^{MQ \times L_1 L_2}$ and $\boldsymbol{B} = (\boldsymbol{B}_{\text{rx}}^{\text{T}} \diamond \boldsymbol{B}_{\text{tx}}^{\text{H}}) \in \mathbb{C}^{N \times L_1 L_2}$ represents the channel geometry information from the BS-UE and IRS, respectively. The collection of matrices $\{\boldsymbol{R}_1, \ldots, \boldsymbol{R}_K\}$, in (21) over all blocks $k \in \{1, \ldots, K\}$ can be arranged as a third-order PARAFAC tensor $\mathcal{R} \in \mathbb{C}^{MQ \times N \times K}$, which can be expanded in terms of a tensor notation as

$$
\mathcal{R} \approx \mathcal{I}_{3, L_1 L_2} \times_1 \boldsymbol{A} \times_2 \boldsymbol{B} \times_3 \boldsymbol{F}^{\text{T}} \in \mathbb{C}^{MQ \times N \times K}, \quad (22)
$$

where $\boldsymbol{F} = [\boldsymbol{f}_1, \cdots, \boldsymbol{f}_K] \in \mathbb{C}^{L_1 L_2 \times K}$ is the combined pathloss across all K blocks. The matrix unfoldings of $\mathcal{R}$ are given by

$$
\begin{aligned}
[\mathcal{R}]_{(1)} &= \boldsymbol{A}\left(\boldsymbol{F}^{\text{T}} \diamond \boldsymbol{B}\right)^{\text{T}} \in \mathbb{C}^{MQ \times NK}, \quad &(23) \\
[\mathcal{R}]_{(2)} &= \boldsymbol{B}\left(\boldsymbol{F}^{\text{T}} \diamond \boldsymbol{A}\right)^{\text{T}} \in \mathbb{C}^{N \times MQK}, \quad &(24) \\
[\mathcal{R}]_{(3)} &= \boldsymbol{F}^{\text{T}}\left(\boldsymbol{B} \diamond \boldsymbol{A}\right)^{\text{T}} \in \mathbb{C}^{K \times MQN}. \quad &(25)
\end{aligned}
$$

Consequently the estimation of $\boldsymbol{A}$, $\boldsymbol{B}$, and $\boldsymbol{F}$ consists of solving the following optimization problem

$$
\left\{\hat{\boldsymbol{A}}, \hat{\boldsymbol{B}}, \hat{\boldsymbol{F}}\right\} = \arg \min_{\boldsymbol{A}, \boldsymbol{B}, \boldsymbol{F}} ||\mathcal{R} - \mathcal{I}_{3, L_1 L_2} \times_1 \boldsymbol{A} \times_2 \boldsymbol{B} \times_3 \boldsymbol{F}^{\text{T}}||_{\text{F}}^2, \quad (26)
$$

which can be performed by means of the ALS algorithm (summarized in Algorithm 1) [12], [16].

Algorithm 1 Alternating least squares

Require: Tensor $\mathcal{R}$, maximum number of iterations $i_{\max}$, convergence threshold δ.
1: Initialize randomly $\boldsymbol{A}$, $\boldsymbol{B}$, and $\boldsymbol{F}$ at iteration $i = 0$.
2: **while** $||e(i) - e(i-1)|| \geq \delta$ and $i < i_{\max}$ **do**
3:      Find a least squares estimate of $\boldsymbol{A}$ as

$$
\hat{\boldsymbol{A}} = [\mathcal{R}]_{(1)} \left[(\hat{\boldsymbol{F}}^{\text{T}} \diamond \hat{\boldsymbol{B}})^{\text{T}}\right]^{\dagger}.
$$

4:      Find a least squares estimate of $\boldsymbol{B}$ as

$$
\hat{\boldsymbol{B}} = [\mathcal{R}]_{(2)} \left[(\hat{\boldsymbol{F}}^{\text{T}} \diamond \hat{\boldsymbol{A}})^{\text{T}}\right]^{\dagger}.
$$

5:      Find a least squares estimate of $\boldsymbol{F}$ as

$$
\hat{\boldsymbol{F}} = \left([\mathcal{R}]_{(3)} \left[(\hat{\boldsymbol{B}} \diamond \hat{\boldsymbol{A}})^{\text{T}}\right]^{\dagger}\right)^{\text{T}}.
$$

6:      Repeat *until* convergence.
7: **end while**
8: **return** $\hat{\mathcal{R}} \approx \mathcal{I}_{3, L_1 L_2} \times_1 \hat{\boldsymbol{A}} \times_2 \hat{\boldsymbol{B}} \times_3 \hat{\boldsymbol{F}}^{\text{T}}$.

A. ALS Channel Parameter Estimation

In this scenario, the algorithm consists of estimating $\boldsymbol{A}$, $\boldsymbol{B}$, and $\boldsymbol{F}$ in an alternating way by iteratively solving the following cost functions

$$
\hat{\boldsymbol{A}} = \arg \min_{\boldsymbol{A}} \left|\left|[\mathcal{R}]_{(1)} - \boldsymbol{A}(\boldsymbol{F}^{\text{T}} \diamond \boldsymbol{B})^{\text{T}}\right|\right|_{\text{F}}^2, \quad (27)
$$

$$
\hat{\boldsymbol{B}} = \arg \min_{\boldsymbol{B}} \left|\left|[\mathcal{R}]_{(2)} - \boldsymbol{B}(\boldsymbol{F}^{\text{T}} \diamond \boldsymbol{A})^{\text{T}}\right|\right|_{\text{F}}^2, \quad (28)
$$

$$
\hat{\boldsymbol{F}} = \arg \min_{\boldsymbol{F}^{\text{T}}} \left|\left|[\mathcal{R}]_{(3)} - \boldsymbol{F}^{\text{T}}(\boldsymbol{B} \diamond \boldsymbol{A})^{\text{T}}\right|\right|_{\text{F}}^2, \quad (29)
$$

with the solutions for (27)-(29) being respectively given by

$$
\hat{\boldsymbol{A}} = [\mathcal{R}]_{(1)} \left[(\boldsymbol{F}^{\text{T}} \diamond \boldsymbol{B})^{\text{T}}\right]^{\dagger} \in \mathbb{C}^{MQ \times L_1 L_2}, \quad (30)
$$

$$
\hat{\boldsymbol{B}} = [\mathcal{R}]_{(2)} \left[(\boldsymbol{F}^{\text{T}} \diamond \boldsymbol{A})^{\text{T}}\right]^{\dagger} \in \mathbb{C}^{N \times L_1 L_2}, \quad (31)
$$

$$
\hat{\boldsymbol{F}} = \left([\mathcal{R}]_{(3)} \left[(\boldsymbol{B} \diamond \boldsymbol{A})^{\text{T}}\right]^{\dagger}\right)^{\text{T}} \in \mathbb{C}^{L_1 L_2 \times K}, \quad (32)
$$

with each solution requiring that

$$
L_1 L_2 \leq NK, \quad L_1 L_2 \leq MQK, \quad L_1 L_2 \leq MQN. \quad (33)
$$

These conditions are necessary to guarantee the existence of the LS estimates of $\boldsymbol{A}$, $\boldsymbol{B}$, and $\boldsymbol{F}$, respectively, by ensuring that the pseudoinverses on Equations (30)-(32) are well defined. The proposed ALS to solve the problem in (26) consists of three iterative and alternating update steps that follow the LS solutions in (30)-(32). The reconstruction error is minimized to a one-factor matrix at each update by fixing the remaining matrices to their previous estimation. This procedure is repeated until convergence, which happens when the reconstruction error of consecutive iterations, given by $e(i) = ||\mathcal{R} - \hat{\mathcal{R}}(i)||_{\text{F}}^2$, achieves $||e(i) - e(i-1)|| \leq \epsilon$ and ϵ is the threshold parameter with $\hat{\mathcal{R}}(i)$ being the estimated tensor fit model at the ith iteration. We initialize the factor matrices randomly, and the convergence threshold is set to $\epsilon = 10^{-5}$.

TABLE I: Computational complexity: LS, KRF, and ALS.

Algorithm	Computational Complexity
LS (17)	$\mathcal{O}(K(MQN)^3)$
KRF [9]	$\mathcal{O}(KMQN)$
ALS (Alg. 1)	$\mathcal{O}(KMQN\text{ALS}_{\text{iter}}(L_1 L_2)^2(1 + \frac{K}{N} + \frac{K}{MQ}))$

B. Computational complexity

In Table I, we describe the computational complexity for the selected benchmark algorithms, the LS at (17), the KRF from [9], and our proposed PARAFAC ALS algorithm. Consider that the pseudo-inverse of a matrix $\mathbf{A} \in \mathbb{C}^{I \times J}$, with $I > J$, and its rank-R singular value decomposition (SVD) approximation have complexities $\mathcal{O}(IJ^2)$ and $\mathcal{O}(IJR)$ [17], respectively. The KRF [9] estimates the combined channel $\boldsymbol{R}_k = \boldsymbol{H}_k^{\text{T}} \diamond \boldsymbol{G}$ by finding estimates of both $\boldsymbol{G}$ and $\boldsymbol{H}_k$ that solves a set of N rank-one approximations using the SVD along K blocks. Regarding the proposed algorithm, the ALS computes 3 pseudo-inverses (30)-(32) along ALS_{iter} iterations until convergence over K blocks.

IV. SIMULATION RESULTS

We evaluate the performance of the proposed tensor-based algorithm by comparing it again with the reference parameter estimation method based on the KRF [9]. The pilot signal matrix $\boldsymbol{Z} \in \mathbb{C}^{Q \times T}$ is designed as a Hadamard matrix, while a discrete Fourier transform (DFT) is adopted for the IRS phase-shift matrix $\boldsymbol{S}$. The angular parameters $\phi_{\text{bs}}^{(l_1)}$ and $\phi_{\text{ue}}^{(l_2)}$ are randomly generated from a uniform distribution between $[-\pi, \pi]$ while the IRS elevation and azimuth angles of arrival and departure are randomly generated from a uniform distribution between $[-\pi/2, \pi/2]$. The fading coefficients $\boldsymbol{\alpha}$ and $\boldsymbol{\beta}_k$ are modeled as independent Gaussian random variables $\mathcal{CN}(0, 1)$. The parameter estimation accuracy is evaluated in terms of the NMSE given as

$$\text{NMSE}(\boldsymbol{R}) = \mathbb{E} \left\{ \frac{\left\| \boldsymbol{R}_k^{(e)} - \hat{\boldsymbol{R}}_k^{(e)} \right\|_{\text{F}}^2}{\left\| \boldsymbol{R}_k^{(e)} \right\|_{\text{F}}^2} \right\}, \qquad (34)$$

where $\hat{\boldsymbol{R}}_k$ is the estimated tensor fit reconstructed with (22) at the eth run, with $E = 10^4$ being the number of Monte Carlo trials. Unless otherwise stated, the system parameters are $\{M = 4, Q = 4, L_1 = 2, L_2 = 2, N = 16, T = 64, K = 5, \text{ and } \delta = 0.75\}$.

In Fig. 3, we evaluate the NMSE performance associated with the estimation of the combined channel $\boldsymbol{R}_k = \boldsymbol{H}_k^{\text{T}} \diamond \boldsymbol{G}$, as a function of the training SNR to compare selected competing algorithms, the classical LS filter as in (17), the state-of-the-art KRF [9], and our proposed solution in Algorithm 1. We observe that the proposed solution in Algorithm 1 outperforms the LS filter and the state-of-the-art KRF [9] algorithms by approximately 10 dB and 7 dB, respectively. Also, this gain is almost independent of the SNR. In the case of the LS, the estimation is worse because this solution does not exploit the intrinsic Khatri-Rao structure of the channel, while the KRF exploits the separability of the channel structure to refine the estimation process a step further than the LS. In contrast, the proposed ALS is an iterative solution that refines the
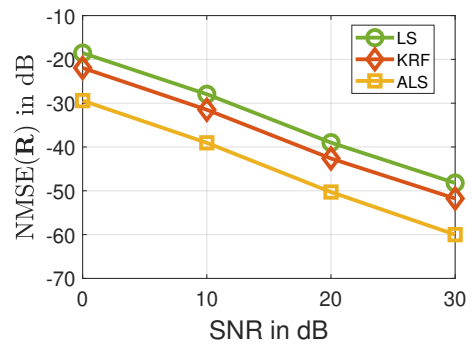

Fig. 3: Performance evaluation in terms of NMSE for the competing algorithms, the LS filter in (17) and the KRF [9], and for the proposed ALS solution in Algorithm 1.
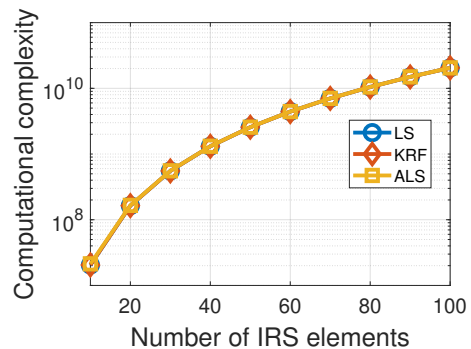

Fig. 4: Computational complexity cost of the competing solutions and the proposed ALS solution in Alg 1 according to the Table I.

estimations until convergence is declared. Furthermore, we also exploit the geometric structure of the scenario in the proposed solution. In all considered methods, we observe that the NMSE decreases with SNR, in the log-domain, linearly as expected.

In Fig. 4, we analyze the computational complexity of the competing algorithms and the proposed solution in Algorithm 1. In this scenario, we fixed all the system parameters except for the number of reflecting elements at the IRS, depicted by N, according to Table I. To compute the cost of the KRF [9], and the ALS in Algorithm 1, we take into account the additional cost from the computation of the combined channel parameters by the LS filter in (17) which is the expensive step of the involved solutions (see Table I). Moreover, simulations show that it takes approximately 10 iterations to achieve convergence in the proposed ALS algorithm. We observe that the competing LS and KRF [9] algorithms have approximately the same cost as the proposed ALS solution.

In Fig. 5a, we evaluate the number of iterations required by the proposed ALS solution in Algorithm 1 to accomplish convergence as a function of the SNR and the number of channel directions, depicted as L_1 and L_2, respectively. We set the target convergence criterion to $\epsilon = 10^{-5}$, which means that convergence is declared when the fit error of the estimated tensor model between consecutive iterations is less than ϵ. As expected, in the low SNR region (< 10 dB), the ALS solution

in Algorithm 1 takes more iterations to declare convergence as the noise variance is higher. Also, when the total number of components, i.e., the product $L_1 L_2$, grows more iterations are needed to solve the problem in (26). On the other hand, at a high SNR regime (> 20 dB), the total number of iterations required for achieving the convergence is considerably lower (around 80% reduction to cases $L_1 L_2 = 2$ and $L_1 L_2 = 3$) however, when $L_1 L_2 = 16$, the proposed ALS algorithm does not achieve the convergence criterion under 100 iterations, i.e., a lower threshold is required or a higher number of iterations at the cost of a higher computational complexity. At the high SNR region (> 20 dB), the required number of iterations is considerably lower than most of the scenarios. However, for the scenario where $L_1 L_2 = 16$ components, the proposed algorithm still has convergence problems under 100 iterations.
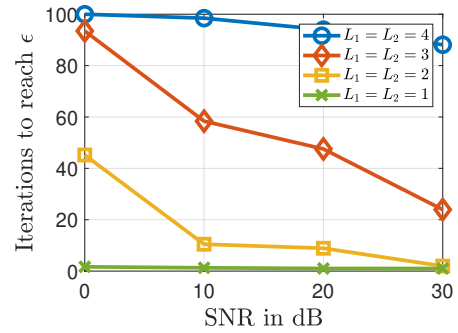
In Fig. 5b, we take the scenario of Fig. 5a for the case where we have $L_1 L_2 = 4$ components and evaluate the impact of the number of reflecting elements of the IRS in the convergence of the ALS solution at Algorithm 1. We observe that, as the number of reflecting elements N increases, fewer iterations are needed for convergence, which is linked to the LS filter in (17) since, if N increases, we can sense the channel longer to achieve a more precise acquisition of the combined channel state information (CSI). Furthermore, we notice that for this scenario, all the cases accomplish the convergence at the high SNR region (> 20 dB) independently of the number of reflecting elements.
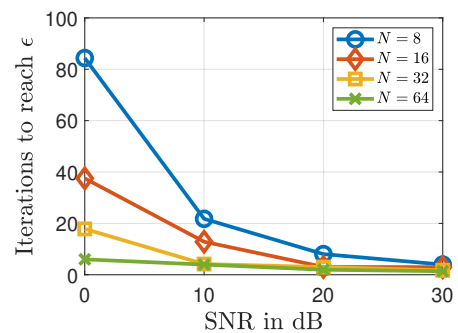
V. Conclusions

This paper proposes a tensor-based channel estimation algorithm for a single time-varying channel in IRS-assisted systems. Different from our work in [10], we considered that the channel BS-IRS remains quasi-static, but the channel IRS-UE has time-varying fading components. In contrast, the parametric structure of the scenario is considered to remain approximately constant. We have proposed a tensor modeling for the reflected signal by the IRS that explores a 3rd order PARAFAC tensor structure. To solve the CSI acquisition in this scenario, we derive an ALS solution according to Alg. 1. The parameter estimation accomplishes the estimation of only the overall channel UE-IRS-BS.

(a) Iterations to converge as function of the SNR for different numbers of paths L_1 and L_2.

(b) Iterations to converge as function of the SNR for different toal IRS elements N.

Fig. 5: Performance evaluation in terms of the required number of iterations for the proposed ALS solution in (1).

References

[1] N. Al-Falahy and O. Y. Alani, "Technologies for 5G networks: Challenges and opportunities," *IT Professional*, vol. 19, no. 1, pp. 12–20, 2017.

[2] N. Ashraf, S. A. Sheikh, S. A. Khan, I. Shayea, and M. Jalal, "Simultaneous wireless information and power transfer with cooperative relaying for next-generation wireless networks: A review," *IEEE Access*, vol. 9, pp. 71482–71504, 2021.

[3] Y. Xu, G. Gui, H. Gacanin, and F. Adachi, "A survey on resource allocation for 5G heterogeneous networks: Current research, future trends, and challenges," *IEEE Communications Surveys & Tutorials*, vol. 23, no. 2, pp. 668–695, 2021.

[4] Q. Wu, S. Zhang, B. Zheng, C. You, and R. Zhang, "Intelligent reflecting surface-aided wireless communications: A tutorial," *IEEE transactions on communications*, vol. 69, no. 5, pp. 3313–3351, 2021.

[5] B. Ji, Y. Han, S. Liu, F. Tao, G. Zhang, Z. Fu, and C. Li, "Several key technologies for 6G: Challenges and opportunities," *IEEE Communications Standards Magazine*, vol. 5, no. 2, pp. 44–51, 2021.

[6] B. Zheng, C. You, W. Mei, and R. Zhang, "A survey on channel estimation and practical passive beamforming design for intelligent reflecting surface aided wireless communications," *IEEE Commun. Surv. Tutor.*, vol. 24, no. 2, pp. 1035–1071, 2022.

[7] C. Pan, G. Zhou, K. Zhi, S. Hong, T. Wu, Y. Pan, H. Ren, M. Di Renzo, A. L. Swindlehurst, R. Zhang, *et al.*, "An overview of signal processing techniques for RIS/IRS-aided wireless systems," *IEEE J. Sel. Topics Signal Processing*, vol. 16, no. 5, pp. 883–917, 2022.

[8] M. Åström, P. Gentner, O. Haliloglu, B. Makki, and O. Tageman, "RIS in cellular networks – challenges and issues," 2024.

[9] G. T. de Araújo, A. L. de Almeida, and R. Boyer, "Channel estimation for intelligent reflecting surface assisted MIMO systems: A tensor modeling approach," *IEEE J. Sel. Top. Signal Process*, vol. 15, no. 3, pp. 789–802, 2021.

[10] K. B. A. Benicio, A. L. F. de Almeida, B. Sokal, Fazal-E-Asim, B. Makki, and G. Fodor., "Tensor-based modeling/estimation of static channels in IRS-assisted MIMO systems," in *2023 Brazilian Symposium on Telecommunications and Signal Processing (SBrT)*, vol. 2023, pp. 1–5, 2023.

[11] K. B. Benício, A. L. de Almeida, B. Sokal, B. Makki, G. Fodor, *et al.*, "Tensor-based channel estimation and data-aided tracking in irs-assisted mimo systems," *IEEE Wireless Communications Letters*, 2023.

[12] P. Comon, X. Luciani, and A. L. de Almeida, "Tensor decompositions, alternating least squares and other tales," *J. Chemom.*, vol. 23, no. 7-8, pp. 393–405, 2009.

[13] R. W. Heath, N. Gonzalez-Prelcic, S. Rangan, W. Roh, and A. M. Sayeed, "An overview of signal processing techniques for millimeter wave MIMO systems," *IEEE J. Sel. Top. Signal Process*, vol. 10, no. 3, pp. 436–453, 2016.

[14] G. Fodor, S. Fodor, and M. Telek, "Performance analysis of a linear MMSE receiver in time-variant Rayleigh fading channels," *IEEE Trans. Commun*, vol. 69, no. 6, pp. 4098–4112, 2021.

[15] B. Makki and T. Eriksson, "Feedback subsampling in temporally-correlated slowly-fading channels using quantized CSI," *IEEE Trans. Commun.*, vol. 61, no. 6, pp. 2282–2294, 2013.

[16] A. L. F. de Almeida, G. Favier, J. da Costa, and J. C. M. Mota, "Overview of tensor decompositions with applications to communications," *Signals and images: advances and results in speech, estimation, compression, recognition, filtering, and processing*, vol. 12, pp. 325–356, 2016.

[17] N. Kishore Kumar and J. Schneider, "Literature survey on low rank approximation of matrices," *Linear and Multilinear Algebra*, vol. 65, no. 11, pp. 2212–2244, 2017.